Point defects in BaSi$_2$ thin films for photovoltaic applications studied by positron annihilation spectroscopy

Montes, A.; Eijt, S. W.H.; Tian, Y.; Gram, R.; Schut, H.; Suemasu, T.; Usami, N.; Zeman, M.; Serra, J.; Isabella, O.

Important note
To cite this publication, please use the final published version (if applicable).
Please check the document version above.

Point defects in BaSi$_2$ thin films for photovoltaic applications studied by positron annihilation spectroscopy

A. Montes (iD), S. W. H. Eijt (iD), Y. Tian (iD), R. Gram (iD), H. Schut, T. Suemasu (iD), N. Usami (iD), M. Zeman (iD), J. Serra (iD), and O. Isabella (iD)

View Online   Export Citation   CrossMark

ARTICLES YOU MAY BE INTERESTED IN

Point defects in BaSi₂ thin films for photovoltaic applications studied by positron annihilation spectroscopy

A. Montes,[1,2,3] (iD) S. W. H. Eijt,[4,a)] (iD) Y. Tian,[1] (iD) R. Gram,[4] (iD) H. Schut,[4] T. Suemasu,[5] (iD) N. Usami,[6] (iD) M. Zeman,[1] (iD) J. Serra,[2,3] (iD) and O. Isabella[1,b)] (iD)

AFFILIATIONS

[1]Photovoltaic Materials and Devices Group, Faculty of Electrical Engineering, Mathematics and Computer Science, Delft University of Technology, Delft NL-2628 CD, The Netherlands
[2]Faculty of Sciences of University of Lisbon, Lisbon 1749-016, Portugal
[3]Instituto Dom Luis, University of Lisbon, Lisbon 1749-016, Portugal
[4]Department of Radiation Science and Technology, Faculty of Applied Sciences, Delft University of Technology, Delft NL-2629 JB, The Netherlands
[5]Institute of Applied Physics, University of Tsukuba, Ibaraki 305-8573, Japan
[6]Graduate School of Engineering, Nagoya University, Nagoya 464-8603, Japan

[a)]Author to whom correspondence should be addressed: S.W.H.Eijt@tudelft.nl
[b)]Electronic mail: O.Isabella@tudelft.nl

ABSTRACT

Barium di-silicide (BaSi₂) is a very promising absorber material for high-efficiency thin-film solar cells, due to its suitable bandgap, high light absorption coefficient, and long minority-carrier lifetime. In this study, we compare the nanostructure, layer composition, and point defects of BaSi₂ thin films deposited by Radio Frequency (RF) sputtering, Thermal Evaporation (TE), and Molecular Beam Epitaxy (MBE), using Doppler Broadening Positron Annihilation Spectroscopy (DB-PAS) depth profiling, Raman spectroscopy, and x-ray diffraction. Our DB-PAS study on thermally annealed RF-sputter deposited and on TE-deposited BaSi₂ layers, in a comparison with high quality BaSi₂ films produced by MBE, points to the presence of vacancy-oxygen complexes and Si or Ba mono-vacancies, respectively, in the (poly)crystalline BaSi₂ films. The degree of near-surface oxidation increases, going from MBE and TE to the industrially applicable RF-sputtered deposition synthesis. The use of a-Si capping layers on the thermally annealed RF-sputtered BaSi₂ films leads to a clear reduction in sub-surface oxidation and improves the quality of the BaSi₂ films, as judged from DB-PAS.

Published under license by AIP Publishing. https://doi.org/10.1063/1.5126264

I. INTRODUCTION

Barium di-silicide (BaSi₂) is a promising absorber material for high-efficiency thin-film solar cells. BaSi₂ has an orthorhombic structure that is stable in ambient conditions, and both constituent elements, silicon and barium, are abundant and of low toxicity. This semiconducting material possesses a suitable bandgap ($E_g \sim 1.3$ eV) for solar energy conversion,[1] a high optical absorption coefficient (α) reaching 10^5 cm^{-1} for photon energies above 1.5 eV,[2] a large minority-carrier diffusion length of $\sim 10\,\mu$m, and a long minority-carrier lifetime $\tau \sim 10-27\,\mu$s.[3] Theoretically, the

attainable conversion efficiency of BaSi₂ homojunction solar cells is $\sim 25\%$[4] and an experimental conversion efficiency of 9.9% has already been reported for p-BaSi₂/n-Si heterojunction solar cells where the BaSi₂ film was grown by Molecular Beam Epitaxy (MBE).[1] MBE-grown samples currently lead to the best solar cell performances, as the resulting BaSi₂ films exhibit the most defect-free structures as judged by Transmission Electron Microscopy (TEM). However, MBE is a costly and time-consuming technique, limiting its applicability in industrial solar cell production processes. Other techniques, such as Thermal Evaporation (TE) and

Radio Frequency (RF) magnetron sputtering, have been used in previous studies to successfully produce BaSi$_2$ thin films.[5–7] Polycrystalline BaSi$_2$ thin films can be synthesized through industrially applicable RF-sputtering processes followed by a post-annealing treatment. Nevertheless, previous research shows that this technology faces relevant issues related to material synthesis and quality control, since the high temperature annealing in the range of 600–700 °C, that is necessary for the crystallization of deposited BaSi$_2$ films, also leads to the appearance of an inhomogeneous and layered structure.[7] Besides, the formation of a sub-surface oxide layer during annealing was observed.[7]

In this study, we apply Doppler Broadening Positron Annihilation Spectroscopy (DB-PAS) as a sensitive, non-destructive technique to examine the presence of open volume defects and local oxidation of the layers in a depth-resolved manner.[8–11] Samples produced by MBE, TE, and RF-sputtering were compared using Raman spectroscopy, x-ray diffraction (XRD), and DB-PAS. The RF-sputtered samples were capped with a-Si layers of varying thickness in order to examine their effectiveness in mitigating oxidation.

II. EXPERIMENTAL

BaSi$_2$ films were deposited on Si(111) substrates using MBE, TE, and RF magnetron sputtering, and an a-Si cap layer was deposited on top of each BaSi$_2$ sample. For the MBE samples, a 20-nm template layer of BaSi$_2$ was first deposited on a Si(111) wafer by reactive deposition epitaxy. Subsequently, Ba and Si were co-evaporated on the BaSi$_2$ template at 600 °C until a thickness of 500 nm was reached. The ratio of $R_{Ba}/R_{Si} = 2.2$ of Ba and Si deposition rates was used in the MBE growth in order to minimize the formation of Si vacancies, leading to p-type BaSi$_2$ films with residual hole concentrations below 10^{16} cm^{-3}.[12] For the TE samples, BaSi$_2$ granulates were melted in a tungsten boat in a vacuum chamber and evaporated by resistive heating. The vapor was deposited on a Si(111) substrate at 600 °C. For the RF-sputtering samples, an RF magnetron sputtering setup (Kurt J. Lesker) was used with a stoichiometric ceramic BaSi$_2$ target (Tosoh). The background pressure was maintained at 0.10 Pa during deposition with Ar gas. Subsequently, a capping layer of a-Si was deposited, following the same procedure as for the BaSi$_2$ film, using a Si target instead of a BaSi$_2$ target. Finally, the RF-sputter deposited BaSi$_2$ films were annealed at 600 °C. All samples were characterized by Raman spectroscopy and x-ray diffraction (XRD) to examine the presence of orthorhombic BaSi$_2$ and other crystalline phases. Raman spectra were acquired by an InVia Raman microscope (Renishaw) with an excitation wavelength of 633 nm and collected under top side illumination of the sample. XRD patterns were determined using an X'Pert Pro x-ray diffractometer equipped with an ultrafast linear semiconductor PIXcel detector, using Cu Kα radiation ($\lambda = 0.154$ nm). The x-ray incidence angle ω was fixed at 0.5°. This small angle of incidence was chosen to maximize the interaction of the x-ray beam with the BaSi$_2$ thin films with thicknesses of up to 1 μm. The presence of open volume defects and the layered structure of the samples was studied by Doppler Broadening Positron Annihilation Spectroscopy (DB-PAS) using the mono-energetic low energy positron beam VEP.[8,10] The momentum windows used to extract the

Doppler S- and W-parameters are, respectively, $p_L < 3.0 \times 10^{-3}$ $m_o c$ and 8.2×10^{-3} $m_o c < p_L < 23.4 \times 10^{-3}$ $m_o c$, with longitudinal momentum $p_L = 2\Delta E/c$ and ΔE the Doppler shift in energy of the detected annihilation γ-ray. The S-parameter is a measure of positron annihilation with valence electrons, which provides sensitivity to the presence of open volume defects such as vacancies or vacancy clusters.[9–11] The W-parameter is a measure of annihilation with (semi-)core electrons, providing chemical sensitivity to the positron trapping site.[9–11] A liquid-nitrogen-cooled high-purity Ge (HPGe) detector with an energy resolution of 1.3 keV was used to determine the energy of the emitted annihilation γ-rays.[13] The Doppler depth profiles collected in the range of 0.1–24 keV were fitted using the VEPFIT software.[10]

III. RESULTS AND DISCUSSION

A. Raman spectroscopy

Figure 1(a) presents the Raman spectra for the RF-sputter, TE, and MBE samples. All the samples show the presence of the five Raman bands characteristic of orthorhombic BaSi$_2$,[7,14] corresponding to the three vibrational modes E$_g$ ($\sim$295 cm^{-1} and $\sim$360 cm^{-1}), F$_g$ ($\sim$276 cm^{-1}, $\sim$355 cm^{-1}, and $\sim$376 cm^{-1}), and A$_g$ ($\sim$486 cm^{-1}), indicating successful deposition of crystalline BaSi$_2$ in the orthorhombic structure that is suitable for photovoltaic applications. The MBE and TE samples, as well as some of the RF-sputter deposited samples, show the presence of two additional but low intensity peaks at $\sim$560 cm^{-1} and $\sim$580 cm^{-1} that could stem from Ba–Si–O phases such as Ba$_3$Si$_5$O$_{13}$, Ba$_2$Si$_3$O$_8$, or BaO–SiO$_2$[15,16] that can also be discerned in some of the collected XRD patterns. The Raman spectra of the TE sample show two additional peaks at around 260 cm^{-1} and 315 cm^{-1} that may arise from BaO–SiO$_2$ and/or Ba$_2$Si$_3$O$_8$[15,16] indicating a higher degree of oxidation than the MBE sample. In turn, RF-sputter deposited samples reveal the presence of a sharp 250 cm^{-1} peak that diminishes with increased thickness of the a-Si cap layer and that can be attributed to the presence of oxides in the sub-surface layer, namely, BaO (242 cm^{-1}),[17] SiO$_2$ (245 cm^{-1}),[18] and/or BaSiO$_3$ (247 cm^{-1}).[19] Moreover, a pronounced Raman peak at 520 cm^{-1} is present in this case, increasing in intensity with thickness of the a-Si cap layer. The presence of this Raman peak is caused by the formation of Si nanocrystals[20] in the top part of the sample or at the interface between the a-Si cap layer and the BaSi$_2$ film, induced by the high temperature thermal annealing at 600 °C required for recrystallization of the BaSi$_2$ layer.[7] For the MBE sample, the synthesis procedure used in our study includes the same processing step as in Ref. 6 to deposit a 5 nm a-Si on top of the BaSi$_2$ film, as evidenced by TEM.[6]

B. X-ray diffraction

Figure 1(b) shows the measured XRD patterns for each type of sample. The dashed lines together with the Miller indices for diffraction peaks of orthorhombic BaSi$_2$ show that in all three samples, the orthorhombic BaSi$_2$ phase is the dominant crystalline fraction, in accordance with the Raman analysis. The MBE sample clearly shows a less polycrystalline character and more preferred orientation than the other samples. We note that, since a grazing incidence XRD geometry (with ω = 0.5°) was used in the present
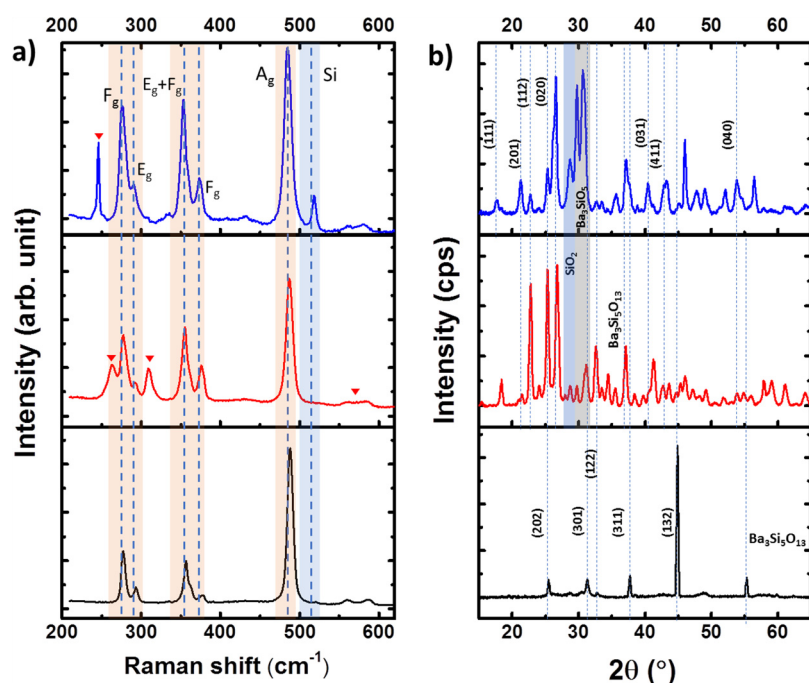
FIG. 1. (a) Raman spectra and (b) XRD patterns of $BaSi_2$ samples deposited by, from top to bottom, RF-sputtering, thermal evaporation, and molecular beam epitaxy.

study rather than a θ–2θ geometry that is suitable to detect preferred orientation, the present $BaSi_2$ film may still exhibit the expected (200), i.e., a-axis, preferred orientation parallel to the sample surface normal as determined in Ref. 12. The additional diffraction peak at $2\theta = 55.5°$ can be attributed to the $Ba_3Si_5O_{13}$ phase. The TE and RF-sputtered samples are clearly more oxidized, as they show additional diffraction peaks that can be linked to Ba–Si–O compounds, such as Ba_3SiO_5, Ba_3Si_5, $Ba_2Si_3O_8$, BaO, SiO_2, and $BaSiO_3$, even when the large majority of diffraction peaks stem from orthorhombic $BaSi_2$. Figure 1(b) shows that SiO_2 is also observed for the TE and RF-sputtered samples, indicative of surface and sub-surface oxidation.

C. Positron annihilation spectroscopy

Subsequently, we applied positron Doppler broadening depth profiling in order to compare the quality of the $BaSi_2$ films and the layered structure of the samples resulting from the MBE, TE and thermally annealed RF-sputter deposition methods. Figures 2(a) and 2(b) show the collected positron Doppler broadening S-parameter and W-parameter depth profiles of the MBE sample as a function of positron implantation energy. In the S and W depth profiles, three regions can be recognized as a function of average depth below the surface, namely, (1) the near-surface region dominated by contributions of the a-Si cap layer and surface annihilation (in blue), (2) the $BaSi_2$ layer (in yellow), and (3) the Si (111) substrate (in green). The apparently gradual (instead of sharp) transition between the layers stems from the spread in depth at which positrons are stopped in the material at a given implantation energy, that approximately follows a Makhovian implantation profile.[9–11] The top layer of this sample consists of

10 nm of a-Si, which is very thin compared with the thickness of the $BaSi_2$ layer of ~500 nm. For this reason, the Doppler depth profiles show a fast transition between the surface value for the S (W) parameter at the lowest energies toward the high S (low W) parameter of the bulk $BaSi_2$ film, which is finally reached at about 5 keV. The S and W values characteristic of the 10 nm thin a-Si layer are thus hidden in the fast change of S and W in the low energy range of 0–1.5 keV. At high energies beyond 5 keV, an increasingly larger fraction of the implanted positrons is stopped in the Si(111) substrate, leading to a gradual transition between the $BaSi_2$ film and the substrate due to the broad Makhovian implantation profiles at high energies.

A good agreement of the VEPFIT analysis using a three-layer model [a-Si, $BaSi_2$ and a semi-infinite Si(111) substrate] and the measured data could be obtained, with S- and W-parameters of the Si(111) that are consistent with extracted values of $S_{substrate} = 0.5681 \pm 0.0003$ and $W_{substrate} = 0.0293 \pm 0.0005$ from independent measurements on bare substrates. In Fig. 2(c), the corresponding S–W diagram is shown, which provides a facile way to identify S–W points of individual layers, since to first approximation most of the S–W points of the depth profiles are positioned on straight lines connecting the S–W points of neighboring layers in the S–W diagram.[10] Figure 2(c) shows that at low energy, most positrons annihilate at the surface leading to a high W and low S-parameter (top-left corner). As the positron implantation energy increases, more positrons annihilate, first, in the a-Si layer, and subsequently, at higher energies, annihilate in the underlying $BaSi_2$ layer, with the S–W data point moving from top-left to the bottom-right corner, at which the S-parameter reaches its maximum value. The S–W point corresponding to annihilation in the $BaSi_2$ layer is represented by the yellow star in the S–W diagram, with
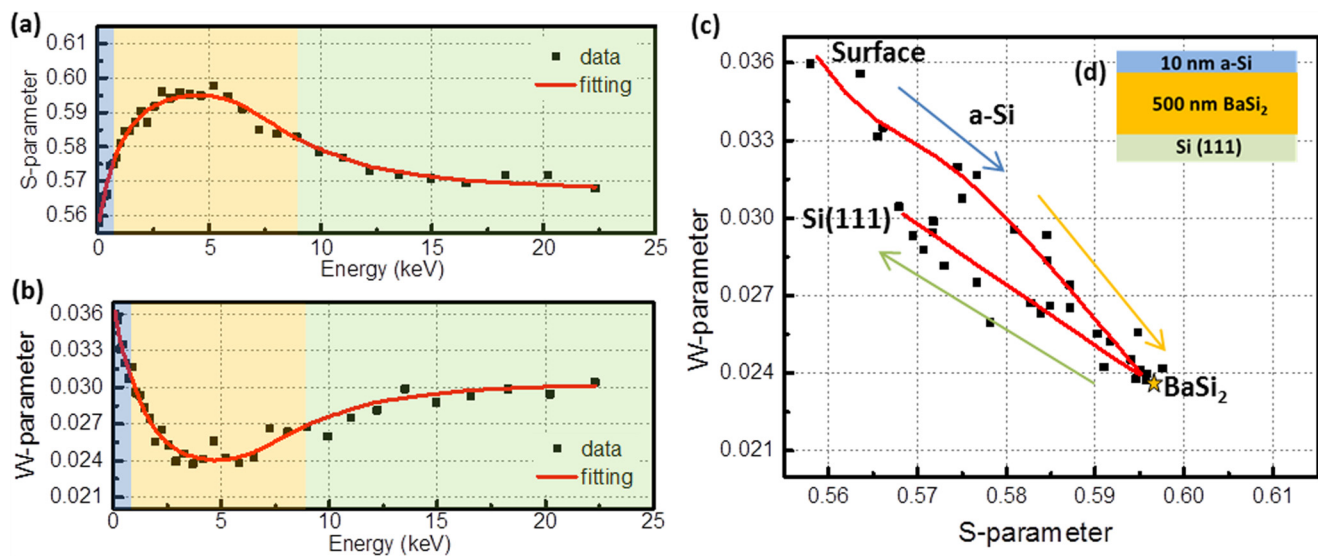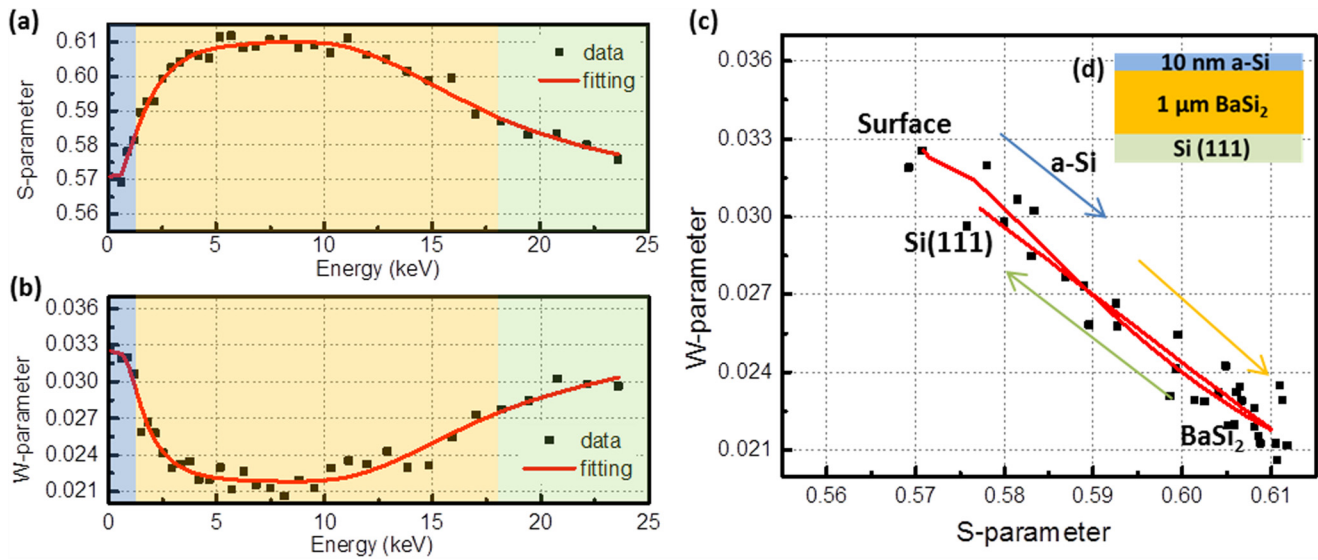
FIG. 2. (a) S-parameter and (b) W-parameter depth profile of MBE-grown BaSi$_2$ on a Si(111) wafer. Full lines are best-fit curves obtained using the VEPFIT program. (c) S–W diagram of MBE-grown BaSi$_2$ on Si(111). (d) Schematic layered structure of the MBE sample. The positron annihilation energy for each boundary was extracted from the VEPFIT analysis and corresponds to the energy where the fractions of positrons annihilating in the two neighboring layers are equal.

$S_{BaSi_2} = 0.596 \pm 0.003$ and $W_{BaSi_2} = 0.0237 \pm 0.0005$ extracted from the VEPFIT analysis. The BaSi$_2$ film produced by MBE is considered to be almost defect-free, since MBE growth of BaSi$_2$ films using R_{Ba}/R_{Si} ratios in the range 2.0–2.6 leads to suppression of Si vacancy formation, with vacancy concentrations well below typical residual hole concentrations of 10^{15}–10^{16} cm^{-3},[12] i.e., below the detection limit of PAS of $\sim 10^{16}$ cm^{-3}.[11] Since the formation energy of Ba vacancies in BaSi$_2$ is generally higher than for Si vacancies in BaSi$_2$,[21] we assume that the MBE-grown BaSi$_2$ film contains a low concentration of Ba vacancies that is not detected by PAS either. We note that a rigorous test of this conjecture requires positron annihilation lifetime studies in combination with *ab initio* calculations.[11,22] In this study, we take the extracted S and W values of the MBE-grown BaSi$_2$ film as reference parameters characteristic for defect-free (high quality) BaSi$_2$ as a comparative tool in the further analysis of the samples produced by the TE and RF-sputter deposition methods.

In Figs. 3 and 4, the same type of analysis was applied to the DB-PAS depth profiles obtained for the thermally evaporated (TE) and the RF-sputtered samples. A similar three-layer structure as for the MBE sample is visible for the TE sample, but quantitative differences are observed. A much broader plateau in the S-parameter and W-parameter depth profiles is present, which results from the larger thickness of ~ 1000 nm for the BaSi$_2$ layer [Fig. 3(d)]. Most importantly, the S-parameter of the TE BaSi$_2$ film is about 2% higher than the reference value deduced from the MBE sample, while the W-parameter has decreased by $\sim 8\%$ (Table I). This suggests the formation of Ba or Si mono-vacancies (and possibly also di-vacancies) in the BaSi$_2$ crystal lattice. In particular, previous studies on c-Si indicate an estimated increase of 3% in S and decrease of 20% in W for mono-vacancies in c-Si compared to

defect-free c-Si, while di-vacancies lead to somewhat larger changes of +4% in S and –25% in W (see Ref. 23 and references therein). Furthermore, *ab initio* calculations indicate moderate formation energies of Si mono-vacancies in BaSi$_2$, in the range of 1.11–1.24 eV for the Si located at 3 inequivalent positions in the BaSi$_2$ unit cell.[12] The moderate formation energies suggest that such Si vacancies in BaSi$_2$ may play an important role in deterioration of the performance of BaSi$_2$ solar cells, as they will lead to the presence of defect states within the bandgap.[12] However, since Si is more electronegative than Ba, it may exhibit a local effectively negative charge in BaSi$_2$, similar to the case of Mg$_2$Si.[24] Si vacancies thus might relatively easily carry a net positive charge, leading to repulsion of the positron and a very small positron trapping probability. Indeed, recent *ab initio* calculations[21] show that the dominant vacancy in BaSi$_2$ is a positively charged Si mono-vacancy under most conditions, while negatively charged Si mono-vacancies may still occur at high Fermi energy conditions. Therefore, the changes in S and W might also be related to the formation of Ba mono-vacancies in the TE BaSi$_2$ film, albeit that the formation energy of V$_{Ba}$ is rather high (in the range of 1.5–3.5 eV according to Ref. 21). Given the typical grain sizes in TE BaSi$_2$ films of 50–100 nm,[25] a minority fraction of positrons trapping and annihilating in grain boundaries may also occur.

Figure 4 shows the Doppler depth profiles collected for two thermally annealed RF-sputter samples, with a-Si capping layers of 10 nm and 50 nm, respectively. The samples were deposited on different substrates; the sample with 10 nm of a-Si was deposited on a Si(111) wafer and the sample with 50 nm a-Si on a Corning glass substrate. The shapes of the depth profiles show pronounced differences, particularly at low energies in the range of up to 3 keV. The

FIG. 3. (a) S-parameter and (b) W-parameter depth profile of TE grown BaSi$_2$ on a Si(111) wafer. Full lines are best-fit curves obtained using the VEPFIT program. (c) S–W diagram of TE grown BaSi$_2$ on Si(111). (d) Schematic layered structure of the TE sample.

S-parameter in this energy range is clearly lower than for all layers of the MBE and TE samples, and it is also much lower than characteristic values for a-Si:H and c-Si layers. The W-parameter, on the other hand, is large. This indicates the presence of an oxide subsurface layer with a thickness of around 70 nm in both cases,

consistent with Auger Electron Spectroscopy (AES) and TEM results obtained in a previous study on thermally annealed RF-sputtered BaSi$_2$ films.[7] This points to the formation of an oxide top layer that consists of SiO$_2$, BaO and Ba–Si–O compounds, in accordance with Raman spectroscopy and XRD (Fig. 1).
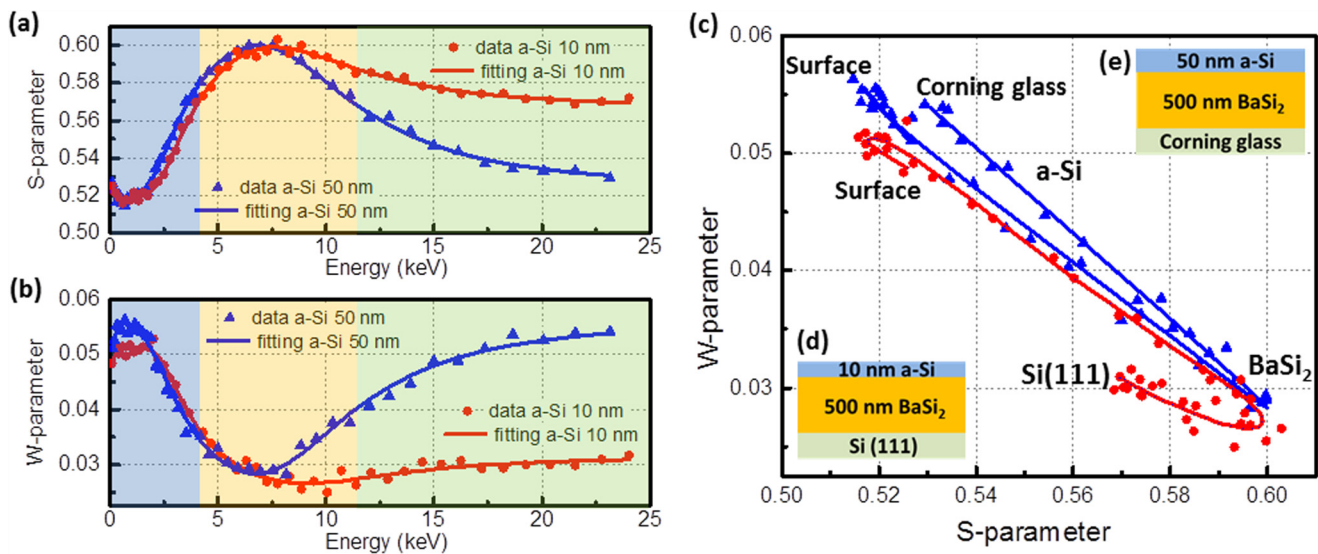
FIG. 4. (a) S-parameter and (b) W-parameter depth profile of two RF-sputtered BaSi$_2$ films capped with, respectively, 10 nm and 50 nm a-Si layers on, respectively, a Si (111) wafer and a Corning glass substrate. Full lines are best-fit curves obtained using the VEPFIT program. (c) S–W diagram of the two RF-sputtered BaSi$_2$ samples. (d) Schematic layered structure of the RF-sputtered samples with a top a-Si layer of 10 nm. (e) Schematic layered structure of the RF-sputtered samples with a top a-Si layer of 50 nm.

TABLE I. Best-fit values of the S- and W-parameters of the BaSi$_2$ films grown by MBE, TE, and RF-sputter deposition extracted using VEPFIT. The S and W values of the MBE BaSi$_2$ film are taken as reference to determine the percentage differences of, respectively, S and W for the BaSi$_2$ layer of the other samples.

Sample	S-parameter	$\Delta S/S_0$ (%)	W-parameter	$\Delta W/W_0$ (%)
MBE deposited	$S_0 = 0.596 \pm 0.003$	…	$W_0 = 0.0237 \pm 0.0005$	…
TE deposited	0.610 ± 0.003	+2.3	0.0217 ± 0.0005	−8
RF-sputtered, 10 nm a-Si	0.589 ± 0.003	−1.2	0.0277 ± 0.0005	+17
RF-sputtered, 50 nm a-Si	0.612 ± 0.003	+2.7	0.0258 ± 0.0005	+9

The depth profiles could be satisfactorily fitted using a three-layer model [oxide top layer, BaSi$_2$ layer, and semi-infinite Si(111) or Corning glass substrate[23]]. The fitted S- and W-parameters for the two BaSi$_2$ layers are given in Table I. The S-parameter of the BaSi$_2$ layer of the sample with 50 nm of a-Si is ∼3% larger than that of the MBE reference layer, i.e., even higher than that of the TE sample. This indicates the formation of more or larger vacancies (vacancy clusters) than that for the case of TE. However, the increase in S is now accompanied by a clear increase in W, indicating the formation of vacancy-oxygen complexes that are characterized by relatively high values of W due to the presence of the neighboring oxygen electron orbitals and correspondingly modified local chemical environment of the positron annihilation site centered at the vacancy.

In the case of the sample with a 10 nm a-Si top layer, the S-parameter of the BaSi$_2$ layer is lower and the W-parameter much higher than that for the MBE reference sample, strongly indicating that compositional changes due to local oxidation and barium diffusion are the dominating factors over the presence of vacancies that are likely present in this case as well. The clear difference with the sample with the 50 nm a-Si top layer shows that the application of a thicker a-Si top layer aids to reduce oxidation of the layers. This is furthermore supported by the strong reduction in intensity of the 250 cm^{-1} Raman peak with thickness of the a-Si top layer and indicates a viable route to mitigate oxidation processes that is essential in order to progress toward industrially applicable synthesis of BaSi$_2$ films for photovoltaic applications. Notably, previous studies showed that the application of (thin) cap layers, such as AlO$_x$ and a-Si, is also beneficial for surface passivation of BaSi$_2$ films and the enhancement of the minority-carrier lifetimes and solar efficiencies.[26,27]

IV. CONCLUSIONS

In conclusion, BaSi$_2$ films deposited by three different techniques, MBE, TE, and RF-sputtering, were compared using Raman spectroscopy, XRD analysis, and positron annihilation spectroscopy. All these deposition methods lead to (poly)crystalline BaSi$_2$ films with thicknesses relevant for future high-efficiency photovoltaic devices. Raman spectroscopy and XRD showed that oxidation of near-surface layers and the formation of Ba–Si–O phases plays an increasingly important role when moving toward films deposited by the industrially applicable RF-sputtering method. Oxidation can be mitigated by the application of suitable cap layers such as a-Si and by tailoring synthesis procedures that remove oxygen from the solar cell processing steps. MBE-grown BaSi$_2$ films present excellent crystallinity and may serve as a benchmark to gauge the presence of open volume defects. Our DB-PAS study shows that TE-deposited and RF-sputter deposited BaSi$_2$ films contain, respectively, Si or Ba vacancies and vacancy-oxygen complexes, which may play an important role in limiting solar cell efficiencies as these may give rise to unwanted defect states within the band gap. PAS can serve as a valuable and highly sensitive tool to monitor the presence and evolution of the vacancies in the development of synthesis pathways for high-efficiency BaSi$_2$-based solar cells. Future Positron Annihilation Lifetime Spectroscopy (PALS) studies and comparison with *ab initio* calculations will be beneficial to quantify defect concentrations and the nature of vacancies in high quality BaSi$_2$ films. Detailed insight into defect formation in BaSi$_2$ films grown by various deposition techniques is important to improve the material quality, constituting a crucial step on the promising road towards high-efficiency BaSi$_2$ solar cells.

REFERENCES

[1]K. O. Hara, Y. Nakagawa, T. Suemasu, and N. Usami, Jpn. J. Appl. Phys. **54**, 07JE02 (2015).
[2]K. Toh, T. Saito, and T. Suemasu, Jpn. J. Appl. Phys. **50**, 068001 (2011).
[3]K. O. Hara, N. Usami, K. Nakamura, R. Takabe, M. Baba, K. Toko, and T. Suemasu, Appl. Phys. Express **6**, 112302 (2013).
[4]T. Suemasu, Jpn. J. Appl. Phys. **54**, 07JA01 (2015).
[5]K. O. Hara, C. Yamamoto, J. Yamanaka, K. Arimoto, K. Nakagawa, and N. Usami, Jpn. J. Appl. Phys. **57**, 04FS01 (2018).
[6]T. Suemasu and N. Usami, J. Phys. D Appl. Phys. **50**, 023001 (2017).
[7]Y. Tian, R. Vismara, S. van Doorene, P. Šutta, L. Vančo, M. Veselý, P. Vogrinčič, O. Isabella, and M. Zeman, ACS Appl. Energy Mater. **1**, 3267–3276 (2018).
[8]S. W. H. Eijt, R. Kind, S. Singh, H. Schut, W. J. Legerstee, R. W. A. Hendrikx, V. L. Svetchnikov, R. J. Westerwaal, and B. Dam, J. Appl. Phys. **105**, 043514 (2009).
[9]P. J. Schultz and K. G. Lynn, Rev. Mod. Phys. **60**, 701 (1988).
[10]A. van Veen, H. Schut, and P. E. Mijnarends, "Depth-profiling of subsurface regions, interfaces and thin films," in *Positron Beams and Their Applications*, edited by P. G. Coleman (World Scientific, Singapore, 2000), pp. 191–225.

[11]R. Krause-Rehberg and H. S. Leipner, *Positron Annihilation in Semiconductors: Defect Studies* (Springer-Verlag, Berlin, 1999).

[12]R. Takabe, T. Deng, K. Kodama, Y. Yamashita, T. Sato, K. Toko, and T. Suemasu, J. Appl. Phys. **123**, 045703 (2018).

[13]W. Shi, M. Theelen, A. Illiberi, N. Barreau, S. J. van der Sar, M. Butterling, H. Schut, W. Egger, M. Dickmann, C. Hugenschmidt, M. Zeman, E. Brück, and S. W. H. Eijt, Phys. Rev. Mater. **2**, 105403 (2018).

[14]T. Sato, H. Hoshida, R. Takabe, K. Toko, Y. Terai, and T. Suemasu, J. Appl. Phys. **124**, 025301 (2018).

[15]Y. Takahisha *et al.*, J. Ceram. Soc. Jpn. **118**, 955–958 (2010).

[16]B. J. A. Moulton *et al.*, Int. J. Appl. Glass Sci. **9**, 510–517 (2018).

[17]B. M. Weckhuysen, G. Mestl, M. P. Rosynek, T. R. Krawietz, J. F. Haw, and J. H. Lunsford, J. Phys. Chem. B **102**, 3773–3778 (1998).

[18]M. Chligui, G. Guimbretière, A. Canizares, G. Matzen, Y. Vaills, and P. Simon (2010), see https://hal.archives-ouvertes.fr/hal-00520823 for more information about the 245 cm^{-1} band in the Raman spectrum of silica.

[19]C. Li, S. Xu, P. Zhang, S. Zhao, D. Deng, and S. Zhuang, J. Exp. Nanosci. **5**, 154–161 (2010).

[20]J. Zi, H. Büscher, C. Falter, W. Ludwig, K. Zhang, and X. Xie, Appl. Phys. Lett. **69**, 200–202 (1996).

[21]M. Kumar, N. Umezawa, W. Zhou, and M. Imai, J. Mater. Chem. A **5**, 25293–25302 (2017).

[22]F. Tuomisto and I. Makkonen, Rev. Mod. Phys. **85**, 1583–1631 (2013).

[23]J. Melskens, A. H. M. Smets, S. W. H. Eijt, H. Schut, E. Brück, and M. Zeman, J. Non-Cryst. Solids **358**, 2015–2018 (2012).

[24]H. Ishii, S. Matsuo, P. Karimov, K. Tanada, and J. Kawai, Phys. Rev. B **71**, 205202 (2005).

[25]K. O. Hara, C. Yamamoto, J. Yamanaka, K. Arimoto, K. Nakagawa, and N. Usami, Mater. Sci. Semicond. Process. **72**, 93–98 (2017).

[26]N. M. Shaalan, K. O. Hara, C. T. Trinh, Y. Nakagawa, and N. Usami, Mater. Sci. Semicond. Process. **76**, 37–41 (2018).

[27]R. Takabe, S. Yachi, W. Du, D. Tsukahara, H. Takeuchi, K. Toko, and T. Suemasu, AIP Adv. **6**, 085107 (2016).